Available online at www.sciencedirect.com

jmr&t Journal of Materials Research and Technology

journal homepage: www.elsevier.com/locate/jmrt

Original Article

Manganese-modified lignin biochar as adsorbent for removal of methylene blue

Xu-Jing Liu [a], *Ming-Fei Li* [a,b,c,*], *Sandip K. Singh* [b]

[a] *Beijing Key Laboratory of Lignocellulosic Chemistry, Beijing Forestry University, Beijing, 100083, China*
[b] *Chemical & Biological Engineering Department, Montana State University, Bozeman, MT, 59717, United States*
[c] *State Key Laboratory of Bio-Fibers and Eco-Textiles, Qingdao University, Qingdao, Shandong, 266071, China*

ARTICLE INFO

Article history:
Received 5 February 2021
Accepted 18 March 2021
Available online 24 March 2021

Keywords:
Adsorbent
Lignin
Mn modified adsorbent
Methylene blue
Adsorption

ABSTRACT

Methylene blue, a prevalent cationic type dye, has been extensively utilized in textile industry. Lignin generates as a byproduct and its utilization is required to add a potential economic benefit of a biorefinery process. Lignin-derived porous biochar, as a promising adsorbent, was propitiously prepared by chemical modification with different oxidation number manganese compounds ($KMnO_4$, $MnSO_4$, and MnO_2). The adsorption capacity of MnO_2-loaded biochar to methylene blue dye was substantially higher relative to original biochar. The maximum adsorption capacity was 248.96 mg/g and removal rate was 99.73%, as compared to 234.65 mg/g and 94.0% for unmodified biochar. In comparison, the decolorization rate of the modified biochar exceeded 95%.

Substantial results showed that methylene blue has a strong binding affinity with MnO_2 modified biochar. Adsorption kinetics was described by a quasi-second order model and methylene blue adsorption isotherm was better fitted by Langmuir model. The research provides a promising way for the removal of methylene blue from wastewater through the manufacture of adsorbent from byproduct of biorefinery process.

© 2021 The Author(s). Published by Elsevier B.V. This is an open access article under the CC BY-NC-ND license (http://creativecommons.org/licenses/by-nc-nd/4.0/).

1. Introduction

Methylene blue, a prevalent cationic type industrial dye [1], has been extensively utilized in textile, printing, leather, and other industries as a biochemical colorant [2]. Exposure to the dye, may severely affect human health, causing symptoms such as nausea, vomiting, and difficulty breathing [3,4]. Long-term exposure of methylene blue can even lead to cancer or genetic mutations in humans and other organisms. How to effectively eliminate or substitute methylene blue has become a significant concern over society and the environment. Methylene blue is a typical organic pollution that originates from drain water. Its removal is straited by using a conventional technique, i.e., photocatalytic performance [5]. Many technologies, including adsorption and biological treatment [6], membrane process [7], solidification [8], photolysis [9], ozonation [10], chemical oxidation [11,12] and electrochemical oxidation [13], are used to eliminate dyes from wastewater. The adsorbing material, on account of its moderate price, easy removal processes, and outbound loading capacity, is extensively used in a sewage treatment. A

* Corresponding author.
E-mail address: limingfei@bjfu.edu.cn (M.-F. Li).
https://doi.org/10.1016/j.jmrt.2021.03.076
2238-7854/© 2021 The Author(s). Published by Elsevier B.V. This is an open access article under the CC BY-NC-ND license (http://creativecommons.org/licenses/by-nc-nd/4.0/).

mass of materials having adsorption capacity, was used for wastewater treatment, such as kaolin [14] and porous activated carbon material [15]. These materials are characterized as excellent candidates [16]. However, due to high production cost, difficulty in regeneration, and long consumption time, these adsorbents are challenging for a wide range of utilization in practical production. Activated carbon has been characterized as an exceptional dye adsorption performance [17]. For example, the activated carbon with a high specific surface area, was prepared by $ZnCl_2$ activation-carbonization, and it has an adsorption capacity of 1193 mg/g for methylene blue [18]. However, substantial challenges remain in improving regeneration capacity, adsorption efficacy, dispersity, and affinity for dyes.

Lignocellulosic biomass material is mainly composed of carbohydrates (cellulose and hemicelluloses) and lignin, in which cellulose is a principal feedstock to produce bioethanol through a biorefinery process. Bioethanol production from lignocellulose includes several steps, i.e., pretreatment, hydrolysis, fermentation, and ethanol distillation [19]. Effective pretreatment is an essential step to increase ethanol yield [20]. There are several pretreatment methods, including dilute acid, alkaline pretreatment, organic solvent and more, known to effectively reduce or remove the lignin content [21]. Lignin, is a highly functionalized aromatic polymer, accounts for 15–30% of dried lignocellulose mass [22]. The utilization of lignin waste released from pretreatment as well as hydrolysate, is an urgent issue for the cleaner production of bioethanol in a biorefinery scenario to reach maximum carbon efficacy. Lignin contains a high amount of carbons [23] relative to polysaccharides in lignocellulosic biomass, which can be a potential source to produce biochar. Conversion of low-value lignin into efficient adsorbent, is an essential and promising strategy for an economical biorefinery.

Lignin is a renewable and high-quality precursor for activated carbon. Lignin derived carbon-based adsorbents have been used to adsorb dyes [24]. The activated carbon rooted in lignin has a relatively high structural order and large micropore volume [25]. Consequently, the recent engineering biochar studies are abundant in the new structure and surface properties of biochar [26]. Due to presence of some metals and glorious adsorption capacity, the modification of some metals with activated carbon impregnated with silver, copper, manganese, and iron, has aroused extensive research interests [27, 28]. Metal-modified lignin composites have a high specific surface area and negative surface charge, which lead to excellent adsorption capacity for methylene blue [29]. For example, ZnO composites supported by biochar show excellent adsorption performance in the process of adsorption of methylene blue [30]. Synthesized Fe_3O_4/lignin nanoparticles by modifying biochar with Fe, which showed low equilibrium time and removal capacity of methylene blue up to 621.52 mg/g [31]. It was reported that manganese modified nano-lignin-based biochar shorted the issues of easy agglomeration, recovery of biochar, improved the material efficacy, enhanced the surface binding ability of the biochar composite, and improved the adsorption capacity of the biochar to methylene blue [32].

Doping of Mn can improve the surface electron transfer [33], and ion exchange functional groups of activated carbon's surface. Highly functionalized active functional groups can significantly improve the binding sites of biochar to metal ions [34]. Researchers [35] reported the synthesis of aqueous manganese oxides with $MnSO_4 \cdot H_2O$ and the analysis showed that the synthesized materials were in amorphous. Increasing surface binding sites and improving agglomeration are the vital properties of a high-value biochar, but related reports have not been addressed. To the best of our studies, the adsorption properties of manganese lignin carbon-based composites for methylene blue, have not been reported.

Therefore, this work provides an approach to transform waste lignin into a high-grade adsorbent for methylene blue. Lignin-derived porous carbon was prepared using a chemical modification of lignin by manganese compounds ($KMnO_4$, $MnSO_4$, and MnO_2). The aperture structure and surface properties of the prepared porous biochar were measured. Different adsorption models were selected to discuss the adsorption feasibility of the prepared porous biochar. The possible mechanism of methylene blue adsorption by biochar rooted in manganese embellished lignin, was proposed. The lignin-derived material showed a high capacity of adsorption, and provided a promising path for the manufacture of adsorbent for methylene blue in sewage treatment.

2. Material and methods

2.1. Materials

Lignin (purity 94%), a pretreatment byproduct during bioethanol production, was provided by a bioethanol mill (Shandong Longlive Biotechnology Co., Ltd, China), which was released from corncob residue during alkali treatment. Methylene blue, $KMnO_4$, and anhydrous $MnCl_2$ were purchased from Macleans, Shanghai. NH_4OH, H_3PO_4 and HCl were provided from Beijing Chemical Co. Ltd., China.

2.2. Preparation of biochar

Lignin was washed with deionized water (18.2 MΩ/cm) to eliminate fines and contaminants, then dried overnight in an oven at 110 °C. Lignin (5 g) was suspended in 50 mL 20 wt/wt % H_3PO_4 solution. It was then dispersed evenly for 12 h before drying at 105 °C. Thereafter, an impregnated mixture was obtained. The immersed sample was carbonized in a muffle furnace at 400 °C for 1 h under air atmosphere. The rate of temperature increase was 5 °C/min. The carbonized sample was grinded, washed, and filtered using a funnel. The solid was washed with 100 mL HCl (1.0 M) solution to eliminate the remained chemicals, followed by washed with deionized water till the filtrate turns to neutral pH. The washed carbonized sample was dried at 100 °C for 24 h. The prepared sample was assigned as A_0.

2.3. Modification of biochar

2 g biochar (A_0) was added to 50 mL of $MnCl_2$ solution (0.002 M). After vigorous stirring (600 rpm) for 6 h, 100 mL $KMnO_4$ (0.02 M) solution was added to the mixture until the suspension turned to dark brown. The suspension was filtered, washed and dried

overnight. The obtained sample was assigned as BC-MnO_2. The reactions of biochar with $KMnO_4$ (0.02 M, 50 mL), $MnCl_2$ (0.02 M, 50 mL), $MnSO_4$ (0.02 M, 50 mL) solutions were also performed by following the similar methods as produced modified biochars and named as BC-$KMnO_4$, BC-MnO_2, and BC-$MnSO_4$, respectively.

The modification mechanism of MnO_2 is as follows:

$$2MnO_4^{2-} + 3Mn^{2+} + 2H_2O = 5MnO_2\downarrow + 4H^+$$

2.4. Characterization

The microscopic surface texture of biochar and modified biochar was examined by employing a field emission scanning electron microscope (Zeiss, German) in which the samples were sprayed with gold. The functional groups were investigated by a Fourier-transform infrared spectroscopy combined with an X-ray photoelectron instrument (Thermo Kalpha), which was used to determine the surface elementals of samples and perform peak fitting. Fourier transform infrared (FTIR) spectra of samples were recorded on a Nicolet IS 10 model FTIR spectrometer with a KBr pellet technique scanned 128 times in the region 4000-400 cm^{-1} with a resolution of 4 cm^{-1}. The X-ray diffraction analysis was tested using an Ultima IV instrument at a face velocity of the sweep 10°/min from 5° to 90°. The deconvolution analysis was performed using XPS peak. The specific surface area and porosity were determined by an automatic specific surface analyzer (Autosorb-iQ) and a porosity analyzer (Mike ASAP2460). Prior to process for surface analysis, samples were degassed under the relative pressure (nitrogen partial pressure) of 10^{-8} at 393.15 K for 6 h. The nitrogen adsorption and desorption experiments were conducted under liquid nitrogen at 77.35 K. The following values of P/P_0 were used in the calculation of specific surface areas: 0.995285 (A_0), 0.994668 (BC-MnO_2), 0.995348 (BC-$KMnO_4$), 0.995040 (BC-$MnCl_2$), and 0.995068 (BC-$MnSO_4$). 0.995285 (A_0), 0.994668 (BC-MnO_2), 0.995348 (BC-$KMnO_4$), 0.995040 (BC-$MnCl_2$), and 0.995068 (BC-$MnSO_4$).

2.5. Batch adsorption experiments

Erlenmeyer flasks containing biochar and methylene blue were oscillated using a shaker (ZWYR-2102C) at 298.15 K. Under the oscillation frequency of 150 rpm for a period until the adsorption saturation times were achieved. The effect of the amount of adsorbent added, contact time, initial concentration of dye solution and pH were analyzed using a single factor test. Different amounts of biochar (3, 5, 8, 10, 15, 20 mg) were mixed with methylene blue solutions to probe the effect of adsorbent addition amounts. The resulting solution was stirred at 298.15 K for 24 h in the dark. Under the same conditions, the effect of pH was studied by modifying the pH of the dye solution from 3 to 12 (adjusted with 0.1 M HCl or 0.1 M NaOH). The pHpzc (point of zero charge) of the adsorbent was measured by gravimetric method. Under abiding adsorbent dosage and solution solubility, the influence of the initial concentration of dye on the removal process was probed by changing the solution concentration (5, 10, 20, 50, and 100 mg/L). To make thorough studies of the effect of contact time of each adsorbent was introduced into methylene blue solutions, the stirring times were 5, 10, 15, 30, 60, 90, 120, 180 min, respectively.

The concentration of filtrate was determined by using a UV spectrophotometer (UV 2310 II) that helps to measure the maximum absorbance. The maximum absorption wavelength of methylene blue was noted at 664 nm. The removal capacity of methylene blue by biochar samples was measured by the following equations:

$$\text{Removal rate: } R = \left(\frac{C_0 - C_e}{C_0}\right) \times 100\% \quad (1)$$

$$\text{Adsorption capacity: } Q_e = \frac{(C_0 - C_e) \times V}{M} \quad (2)$$

where, C_0 and C_e representative the initial and equilibrium concentrations of methylene blue solution (mg/L), respectively. M is the indication of the quality of the adsorbent (g) and V represents the volume of the solution (L) [36].

2.6. Adsorption kinetics studies

The adsorption kinetics studies of methylene blue by biochar samples, were investigated via the earlier-mentioned parameters. A specific count of samples was introduced into a 250 mL erlenmeyer flask and mixed with 50 mL methylene blue solution (50 mg/L). The experimental process was carried out at 298.15 K at 150 r/min frequency. The filtrate was disclosed at different adsorption time intervals. Regarding to the adsorption kinetics, pseudo-first-order kinetic model and pseudo-second-order kinetic models were used to probe the adsorption capacity of methylene blue onto each adsorbent surface. Pseudo-first/second-order kinetic models were determined using following equations.

Pseudo-first-order kinetic model:

$$q_t = q_e(1 - e^{-k_1 t}) \quad (3)$$

Pseudo-second-order kinetic model:

$$q_t = \frac{k_2 q_e^2 t}{1 + k_2 q_e t} \quad (4)$$

where k_1 (min^{-1}) and k_2 ($g \cdot mg^{-1} \cdot min^{-1}$) were respectively the rate constants of two models which mentioned earlier. Besides, q_t ($mg \cdot g^{-1}$) and q_e ($mg \cdot g^{-1}$) stand for the values for adsorption performance [37].

2.7. Adsorption isotherm studies

The adsorption process was proceeded in an erlenmeyer flask with predetermined amounts of sample that introduced into 50 mL different concentration methylene blue solutions in the range from 5 to 50 mg/L. The resulting mixture was placed in a shaker (150 rpm) at 298.15 K for 24 h. Thereafter, the supernatant was taken to determine the concentration at equilibrium condition (C_e). The isotherm studies were depicted by using Langmuir and Freundlich adsorption isotherm models. Langmuir and Freundlich adsorption isotherm models are shown as below:

Langmuir adsorption isotherm model:

$$\frac{C_e}{q_e}=\frac{1}{q_m}C_e+\frac{1}{q_m k_L} \quad (5)$$

where q_m ($mg\cdot g^{-1}$) and q_e ($mg\cdot g^{-1}$) depicts the saturated adsorption capacity and equilibrium adsorption capacity severally, k_L ($mg\cdot L^{-1}$) is the adsorption constant, which reflect the degree of adsorption capacity [38]. Using this equation, the values of k_L and $1/q_m$ were calculated from the slope and intercept of the plot of C_e/q_e versus C_e, respectively [39].

Freundlich adsorption isotherm model:

$$lnq_e=\frac{1}{n}lnC_e+lnk_F \quad (6)$$

where k_F ($mg\cdot g^{-1}$ $(L\cdot mg^{-1})^{1/n}$) is the representation of the Freundlich constant. Furthermore, n is intensity of adsorption, which illustrates the adsorption strength [40].Using this equation, the values of k_F and 1/n were calculated from the slope and intercept of the plot of lnq_e versus lnC_e, respectively [36].

3. Results and discussion

3.1. *Characterization of adsorbents*

3.1.1. *FT-IR*

Biochar (A_0) was synthesized by using a chemical activation method, and lignin-derived porous biochars were successfully prepared by a chemical modification of manganese compounds ($KMnO_4$, $MnSO_4$, and MnO_2). FT-IR spectra of the A_0 and BC-MnO_2, BC-$MnSO_4$, and BC-$KMnO_4$ are given in Fig. S1. The lignin-based biochar prepared has abundant functional groups on the surface, containing both aromatic and aliphatic hydrocarbons. The absorption peak ~ 3442 cm^{-1} is attributed to the stretching vibration of hydroxyl groups (-OH) [41]. The peaks ~1620 cm^{-1} is presumed to C–H stretching mode of aromatic ring. The peak ~1384 cm^{-1} reveals the symmetric bending vibration of $-CH_2$ and $-CH_3$. The absorption peak ~ 1262 cm^{-1} represents the characteristic absorption peak of ether bond. The absorption peak ~ 1082 cm^{-1} belongs to the stretching vibration of the carbon–oxygen bond in ether bond. Compared with unmodified biochar A_0, the intensity of the absorption peak of modified biochar was reduced, mainly because carbon–carbon bonds and ether bonds were the main linkages that are present in lignin structure. The bond energy of the ether bonds is less relative to carbon–carbon bond, and ether bonds were more likely to easily cleave when heated [42]. The vibration peaks below 600 cm^{-1}, indicated the tensile vibration caused by the compounds formed with metal ions.

3.1.2. *Characterization of morphological structure*

The pore size and distribution of samples were analyzed via nitrogen adsorption–desorption method and the isotherms are shown in Fig. 1a and b, and Table 1. These four biochar samples pertain to a typical IV isotherm with different BET specific surface areas [43]. A_0 and modified biochar samples had similar pore diameter distributions (Fig. 1 (b)), and the

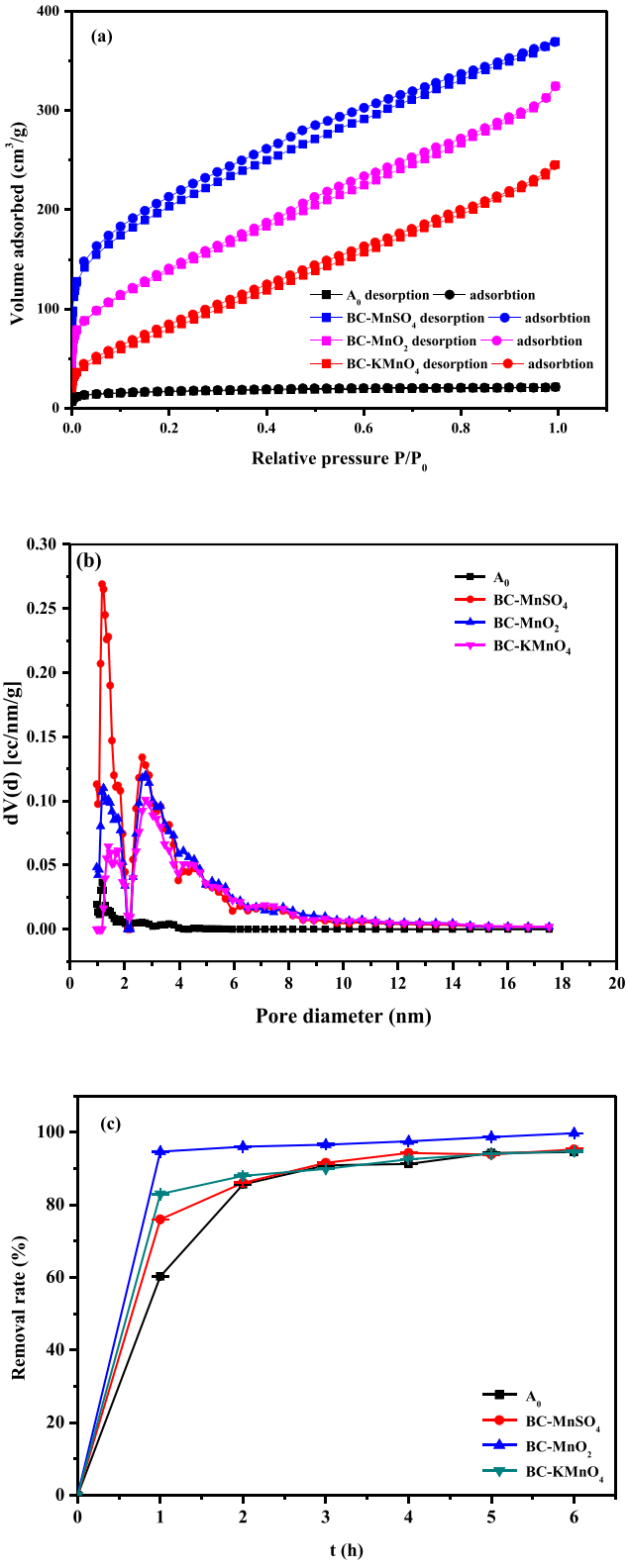


Fig. 1 – (a) N_2 sorption isotherm and (b) pore size distribution (desorption) curve A_0 and BC-MnO_2, BC-$MnSO_4$, and BC-$KMnO_4$, and (c) effect of adsorption–desorption equilibrium time.

Table 1 – Aperture features and surface area values of biochar among modified and unmodified biochars.

Sample	S_{BET} (m^2/g)	Average pore size (nm)	Mesopore volumes (cm^3/g)	Pore volume (cm^3/g)	Pore width (nm)
A_0	48.136	2.184	0.027	0.029	1.178
BC-MnO_2	349.646	3.892	0.336	0.447	2.769
BC-$MnSO_4$	547.234	3.129	0.472	0.520	1.178
BC-$KMnO_4$	186.328	4.434	0.240	0.342	2.769

pore diameters were 0.5–2 nm, indicating that the biochar samples had micropores structure, which can be a beneficial for improvement in adsorption capacity. As shown in Table 1, the pore volume and specific surface area of A_0 were 0.029 cm^3/g and 48.136 m^2/g, respectively. Furthermore, the specific surface area and pore volume of biochar increased obviously after modification. After the modification with $MnSO_4$, the specific surface area of the original biochar was much enlarged, and the pore volume and average pore diameter were also increased, due to dispersion of $MnSO_4$ into the pores of the original biochar through dissociation. Thus the pore density on surface was improved. Compared with BC-$MnSO_4$, the specific surface area and pore volume of BC-MnO_2 were reduced to 349.646 m^2/g and 0.447 cm^3/g, respectively. The analysis suggests that manganese oxide scattered in the micropores and mesopores blocks part of the pores, leading to reduced specific surface area and pore volume of micropores [33]. Specially, due to strong oxidation of $KMnO_4$, the modification with $KMnO_4$ significantly reduced the pore volume and specific surface area. Besides, the average pore size was slightly increased and resulted in the collapse of some microspore structures [34].

3.1.3. *Effect of adsorption–desorption equilibrium time*

The adsorption of activated carbon in methylene blue solution, is a dynamic and continuous reaction process, i.e., adsorption and desorption reach equilibrium for a certain time. The adsorption–desorption of methylene blue dye was carried out using a fixed amount of unmodified biochar (A_0) and modified biochar (BC–$KMnO_4$, BC-MnO_2, and BC-$MnSO_4$) under dark conditions. The known amounts of samples were taken in a 50 mL dye solution (0.16 mM). The dye solution was centrifuged at an interval of 1 h before measuring the absorbance of the solution. The adsorption–desorption equilibrium time results of biochar are mentioned in Fig. 1 (c). During the whole adsorption process, the significant variation of biochar desorption efficacy was observed over time. It can be observed that under the same adsorption time, the adsorption rate of biochar has marked a substantial difference. In the first hour of adsorption, the adsorption rate of unmodified biochar was much lower than that of modified biochar. The decolorization rate was unchanged after 3 h, which can be considered as maximum absorption limit. Under equilibrium conditions, the decolorization rate of the unmodified biochar (A_0) reached about 94.0% and the maximum adsorption capacity was 234.65 mg/g. In comparison, the decolorization rate of the modified biochar exceeded 95%, the maximum adsorption capacity of BC-$KMnO_4$ and BC-$MnSO_4$ were 241.35 mg/g and 237.82 mg/g, among which the decolorization rate of BC-MnO_2 reached up to 99.7%.

3.1.4. *Analysis of surface and structure of BC-MnO_2*

Since the BC-MnO_2 biochar showed the best adsorption capacity, the structure and adsorption capacity analyzed further concentrated on it. The micrographs of these samples showed that the surface morphology of the original biochar changed significantly after modification. A_0 sample showed a highly developed small pore structure with uniform, smooth, and dense texture. On the contrary, for the MnO_2 treated samples, the surface morphology of BC-MnO_2 changed, and its surface was relatively rough with noticeable fine particles attached, and a small portion of gray–white impurities were distributed around it. It is indicated that the surface grain structure of BC-MnO_2 was prominent, and MnO_2 was almost uniformly deposited on the surface. The enhanced adsorption performance of biochar may be related to MnO_2 covered on the surface of biochar.

X-ray diffraction was applied to represent the materials and lignin-derived biochar. It can be presented that the XRD pattern of lignin showed prominent diffraction peaks at 2θ of 15°–23°, indicating that lignin raw materials contained a rich polycrystalline structure [44]. A_0 and BC-MnO_2 showed two substantial diffraction peaks around 2θ of 25° and 43°, respectively, corresponding to graphite's (002) and (100) diffraction peaks [45]. The 002 plane represents as a narrow peak, with a steep rise. Besides, a broad, small diffraction peak appeared on the 100 plane. These properties indicate that A_0 and BC-MnO_2 were dominated by amorphous carbon structure [46]. For BC-MnO_2 sample, the diffraction peaks at 2θ of 37.07° and 42.54° indicated the presence of MnO_2 [43]. These results confirmed that MnO_2 was successfully formed in the surface pores of biochar during the modification process.

XPS spectroscopy was used to examine the surface characteristics of the original biochar and modified biochar (Fig. 2). A noticeable heighten of Mn (2p) was traced out from the spectra of sample after modifying the original biochar by MnO_2. After modification of original biochar by MnO_2, BC-MnO_2 showed a significant increase in Mn (2p) strength. The binding energy of Mn (2p) was within the range of 641.7–642.0 eV [34], and Mn2p3 peak confirmed the existence of MnO_2 at 642 eV. It was revealed that BC-MnO_2 was composed of multiple phases, including manganese oxide and biochar. The spectral intensity of O1s after MnO_2 treatment, was also significantly increased (Fig. 2 (a)). Three components are considered to constitute the corresponding chemical displacement of C1s of A_0, and the binding energies of C–C, C–N, and O–C=O (carboxyl or ester group) are 284.4 eV, 286.0 eV, and 288.4 eV, respectively [47] (Fig. 2 (b)). It was found that the O1s spectrum of A_0 showed two peaks at 531.6 and 531.1 eV, representing for oxygen atoms in the carbonyl group and oxygen atoms in the hydroxyl group or the ether (Fig. 2 (c)). For BC-MnO_2, the O1s spectrum was divided into three

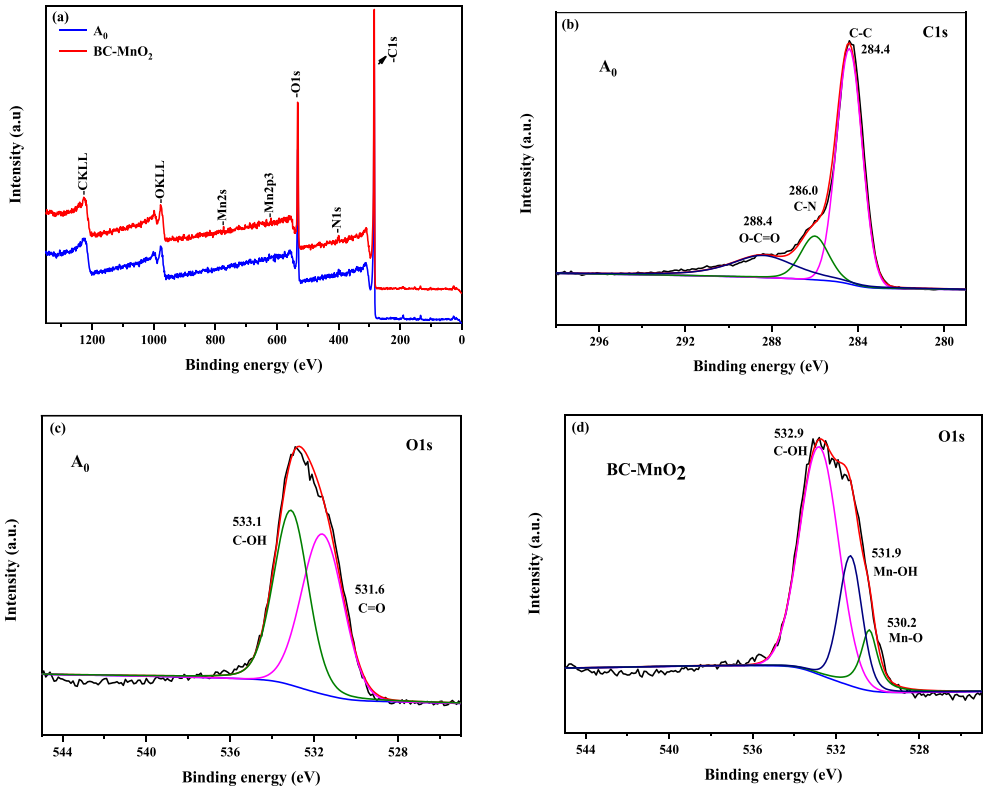


Fig. 2 – (a) XPS survey of A_0 and BC-MnO_2, (b) high-resolution spectra showing O1s and C1s core level in A_0, and (c) high-resolution spectra O1s showing Mn2p core level in BC-MnO_2 along with its deconvolution.

peaks: 530.2, 531.9, and 532.9 eV, respectively (Fig. 2 (d)). They were belonged to metallic oxide (Mn–O) [48], hydroxyl groups bonded with manganese (Mn–OH) [34], and C=O groups on the surface of BC-MnO_2. It can be observed that the oxygen on the surface of biochar was mainly bound to manganese in the form of Mn–O and Mn–OH, which provided vast opportunities for methylene blue dye adsorption.

3.2. *Adsorption performance of adsorbents*

3.2.1. *Effect of pH on adsorption*

Initial pH has a crucial effect in the adsorption efficacy of adsorbing materials on account of the presence of functional groups on the adsorbent surface and the surface charge.-Fig.3(a) illustrated the methylene blue removal efficacy and adsorption capacity of BC-MnO_2 at a series of pH values. Removal efficiency and adsorption capacity also increased with the increment of pH. The removal efficiency of methylene blue was low ~ 77% at pH 2. As the pH of the methylene blue dye reached 11, the adsorbability approached to ~100%, the maximum adsorption capacity reached 248.96 mg/g. The surface of biochar contains chemical groups such as–OH and –COOH, and the pH of the dye altered the charge and electric quantity of these groups [49]. Under acidic conditions, the capacity of H^+ ions combined binding sites on biochar was restricted, while methylene blue was a positively charged cationic dye [50], which was also positively charged. That would lead to the electrostatic repulsion between methylene blue and BC-MnO_2, thus reducing adsorption capacity was characterized. Therefore, it was unable to show the adsorption of methylene blue by BC-MnO_2 at low pH. At higher pH, hydrogen ion competition becomes less critical in the alkaline environment, and electrostatic attraction was enhanced with the heightening of negative charge on the adsorbent surface between BC-MnO_2 and methylene blue molecules [51].

Besides, the curve of the pH_{zppzc} (point of zero charge) of BC-MnO_2 shown in Fig. S4 indicated that the pH_{pzc} value of BC-MnO_2 was 3.4. Thus, at pH < pH_{pzc}, the surface of the adsorbent was positively charged due to protonation, while at pH > pH_{pzc}, the surface of the adsorbent got negatively charged due to deprotonation. Meanwhile, methylene blue is a cationic dye, therefore, electrostatic repulsion occurred between the cationic dye and the positive load on the adsorbent surface, resulting in a decrease in adsorption efficiency. However, under the condition of pH > pH_{pzc}, the electrostatic attraction between the negative surface charge of adsorbents and the positive charge of methylene blue molecules, which resulted in high removal efficiency. This was consistent with the results in Fig. 3(a).

3.2.2. *Effect of biochar addition amount on adsorption*

The effect of biochar amount addition on the adsorption of methylene blue solution, was determined by adsorption of fixed dye concentration (0.16 mM) from 3 to 20 mg of BC-MnO_2 at room temperature in dark (Fig. 3(b)). For BC-MnO_2, the increase of adsorbent dosage led to the increase of methylene blue adsorption removal rate. This was attributed to a higher number of adsorption sites. When the addition of

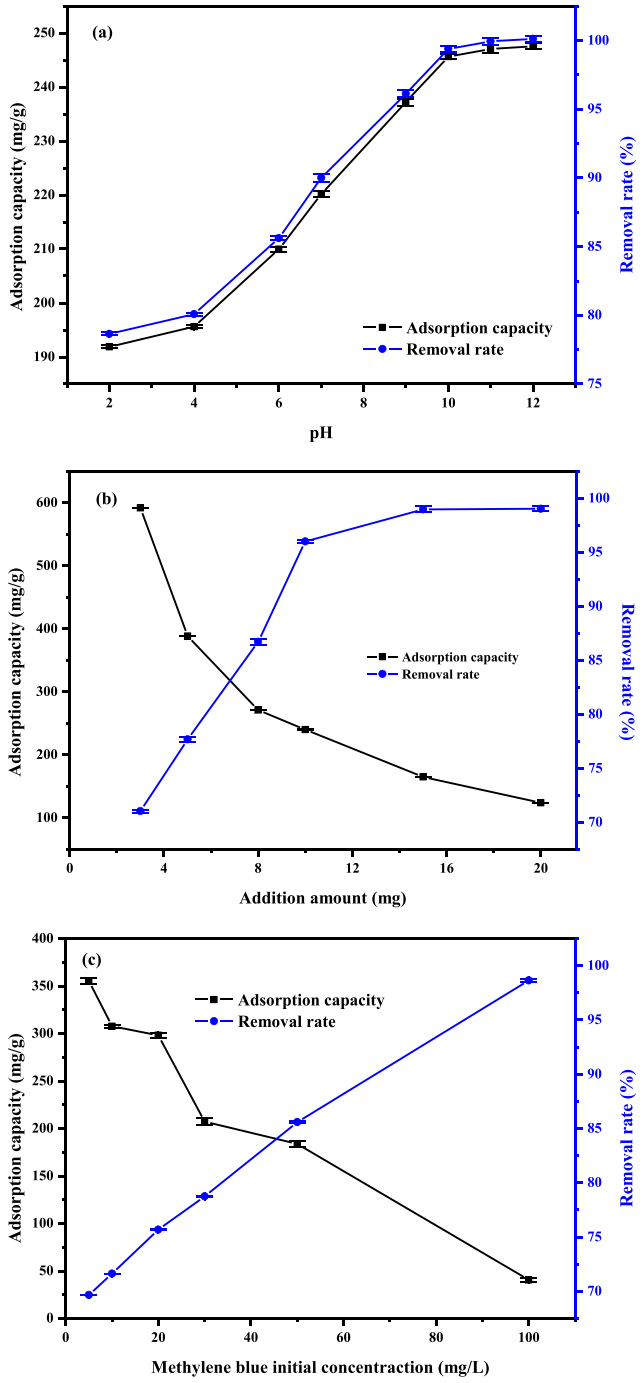


Fig. 3 – (a) Effect of initial concentration of methylene blue solution on adsorption, (b) effect of biochar addition amount on adsorption, and (c) effect of pH on adsorption.

$BC\text{-}MnO_2$ was 3 mg, the equilibrium adsorption capacity of biochar to methylene blue was 591.9 mg/g, with 71.03% removal rate. The adsorption capacity of activated carbon to methylene blue, was 123.8 mg/g at addition amounts of 20 mg $BC\text{-}MnO_2$, and removal rate was 99.05%. The concentration of methylene blue in the system was high at low amounts of $BC\text{-}MnO_2$, and there were many active sites for adsorption, thus the adsorption capacity was high. However, as addition amount continued to increase, the removal rate tended to increase with the increase of dose due to the increase of vacancy adsorption sites availability. However, the removal rate did not increase at the adsorption of methylene blue reached saturation, even if the amount of adsorbent increased.

3.2.3. *Effect of initial concentration of methylene blue solution on adsorption*

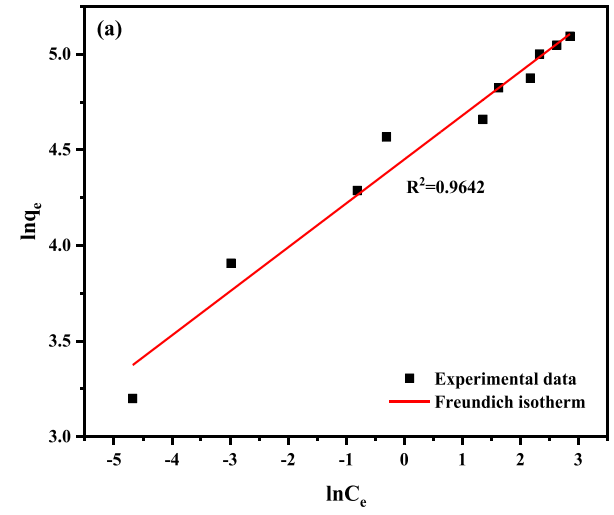
The removal efficacy of methylene blue was investigated based on the influence of initial concentration. $BC\text{-}MnO_2$ was used to conduct batch adsorption studies at predetermined concentrations from 5 to 100 mg/L, and the findings were shown in Fig. 3(c). The adsorption and removal rate of methylene blue solution over $BC\text{-}MnO_2$, reached 98.6% at the beginning (Fig. 3(c)). However, the removal rate decreased as initial concentration increases, because of the reduced active sites required for high concentrations of dyes [52]. Conversely, the adsorption capacity increased rapidly due to high solution concentration and the high adsorption impetus, which ensured the full contact between the adsorbent and methylene blue dye. The adsorption capacity reached 355.96 mg/g at absorbability of 100 mg/L methylene blue solution, and the removal rate reached around 71.03%. It can be considered that the adsorption of methylene blue dye by $BC\text{-}MnO_2$, was close to the adsorption equilibrium when the initial concentration was 100 mg/L. The adsorption could lose its meaning if the removal rate was too low. Therefore, the adsorption capacity did not increase indefinitely.

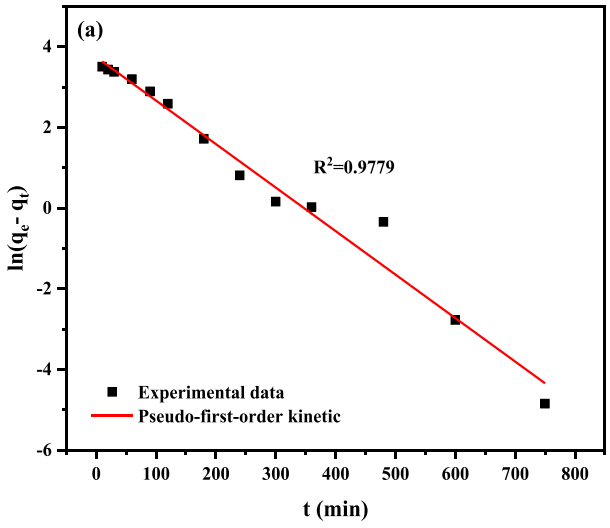
3.2.4. *Adsorption isotherm experiment*

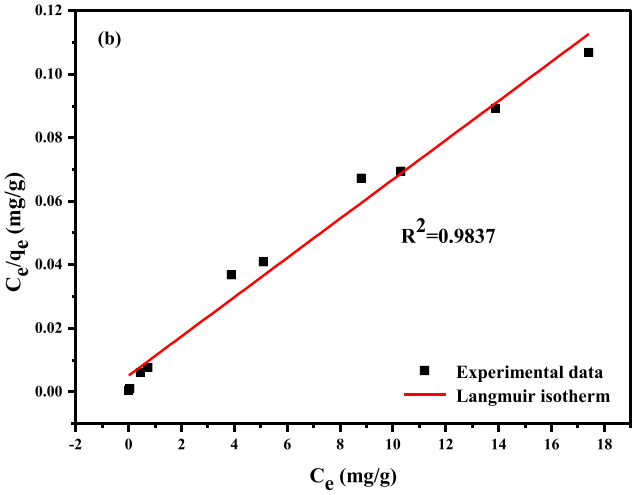
To understand the interaction between the adsorbent and biochar at the equilibrium state, Langmuir and Freundlich isotherms were used to fit with experimental data, as shown in Fig. 4. The isotherm model parameters were determined by regression analysis of experimental data, as shown in Table 2. According to Fig. 4 and Table 2, among Langmuir and Freundlich isothermal models used in this study, the correlation coefficient of the Langmuir model in the adsorption process of methylene blue on $BC\text{-}MnO_2$, was higher than that of the Freundlich model. Furthermore, the theoretical equilibrium adsorption amount obtained by Langmuir isothermal fitting, was 161.81 mg/g, that was near to the equilibrium adsorption amount measured in the experiment. Therefore, it can be concluded that the Langmuir isotherm model can comprehensively and accurately describe the adsorption process of methylene blue in water by $BC\text{-}MnO_2$, that is uniform adsorption point positions on the surface of $BC\text{-}MnO_2$. In literature, similar isotherm results (Table 2) were obtained for various adsorbate–adsorbent systems [53-55]. The methylene blue adsorption process in water, was mainly single-molecular layer adsorption [56]. This result is in line with the results of removing methylene blue from crop straw biochar [57].

3.2.5. *Adsorption kinetics study*

The adsorption mechanism of $BC\text{-}MnO_2$ was determined using a pseudo-first-order kinetic and a pseudo-second-order kinetic models to fit experimental data [43]. In pseudo-first-order kinetic fitting, although the linear fitting result was a relatively straight line, significant deviations can be observed in the







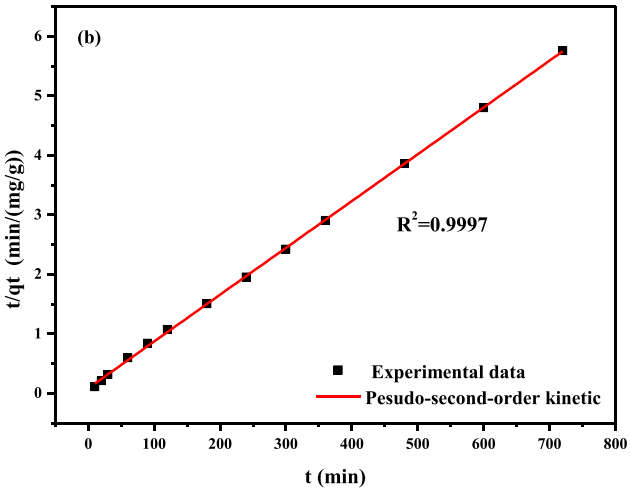


Fig. 4 – (a) Freundlich isotherms and (b) Langmuir isotherms for methylene blue adsorbed by BC-MnO_2.

Fig. 5 – (a) Pseudo-first-order kinetic and (b) Pseudo-second-order kinetic for methylene blue adsorbed by BC-MnO_2.

equilibrium adsorption capacity and experimental adsorption capacity of equation fitting theory (Fig. 5(a)). In contrast, the linear fitting effect of the pesudo-second-order dynamic model was excellent in the case of no significant deviation between the experimental (162.93 mg/g) and the calculated q_e (167.06 mg/g) (Fig.5 (b)). As shown in Table 3, the correlation coefficient (R^2) was 0.9997 for fitting the adsorption process of biochar under different initial methylene blue concentrations using the pseudo-second-order kinetic equation. Therefore, it can be concluded that the pseudo-second-order kinetic model can more accurately describe the kinetic effects of methylene

Table 2 – Langmuir and Freundlich equation fitting parameters of methylene blue adsorbed by BC-MnO_2.

Models	Parameters	
Langmuir isotherm	q_m (mg·g^{-1})	161.81
	k_L (mg·L^{-1})	1.2094
	R^2	0.9837
	SD	0.0529
Freundlich isotherm	k_F (mg·g^{-1} (L·mg^{-1})$^{1/n}$)	85.570
	N	4.3529
	R^2	0.9642
	SD	0.1135

Table 3 – Adsorption kinetics models of methylene blue adsorbed by BC-MnO_2.

Models	$q_{e,exp}$ (mg·g^{-1})	Parameters	
Pseudo-first-order kinetic	162.93	q_e (mg·g^{-1})	42.31
		k_1 (min^{-1})	0.0108
		R^2	0.9779
		SD	0.4457
Pseudo-second-order kinetic	162.93	q_e (mg·g^{-1})	167.06
		k_2 (× 10^{-4}) (g·mg^{-1}·min^{-1})	7.3237
		R^2	0.9997
		SD	0.0317

Table 4 – Adsorption capacities of methylene blue for different adsorbents.

Adsorbent	Adsorption capacity (mg/g)	Reference
Mesoporous limestone	34.24	[61]
Polydopamine microspheres	90.7	[62]
Amorphous adsorbent	53.79	[63]
Rice husk	40.6	[64]
ZnO–NR–AC	89.29	[40]
MXene/sodium alginate gel beads	92.17	[65]

blue in BC-MnO_2 adsorption solution. In literature, similar kinetic results were reported for the adsorption kinetic of various water pollutants by carbon-based adsorbents [53,58,59]. This can be possibly explained that the methylene blue adsorption process of BC-MnO_2 to water, was mainly controlled by the chemisorption mechanism rather than by material transport step [60]. Biochar produced by pyrolysis of banana pseudostem [61] and fallen leaf [62], has similar theory on adsorption of methylene blue solution. BC-MnO_2 is a potential candidate to remove methylene blue dye from aqueous solution, which is higher than mesoporous limestone [63], polydopamine microspheres [64], amorphous adsorbent [65], rice husk [66], ZnO–NR–AC [40], and MXene/sodium alginate gel beads [67], as shown in Table 4.

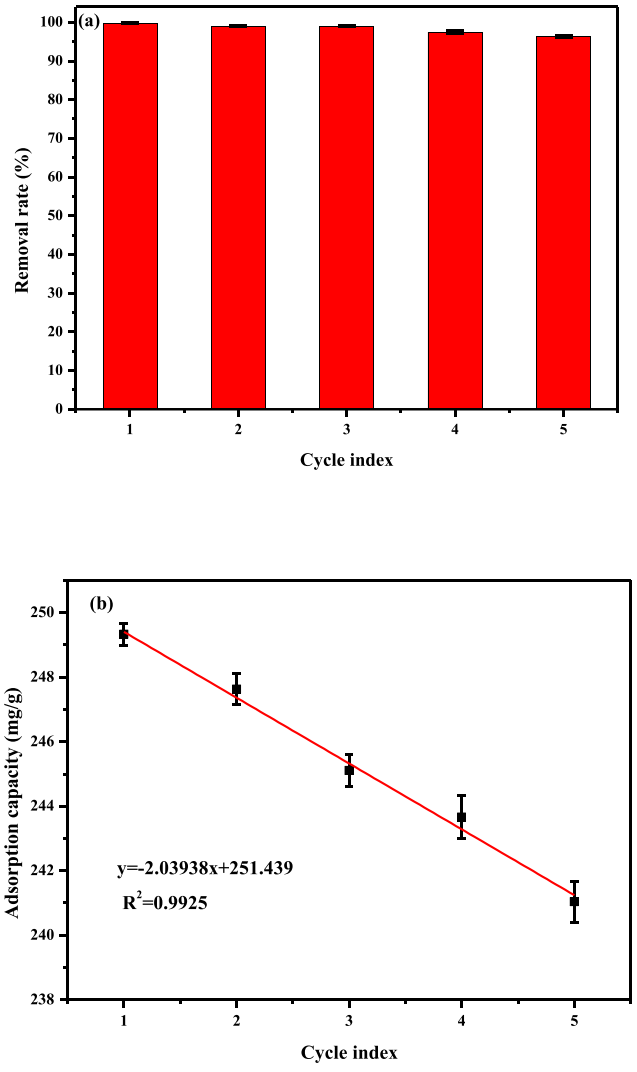


Fig. 6 – (a) The removal rate and (b) adsorption capacity of BC-MnO_2 for methylene blue adsorption throughout five consecutive cycles of reuse.

3.2.6. *The regeneration of adsorbent*

To measure whether adsorbent could be recycled for use, the material prepared for adsorption of methylene blue was recovered simply by filtering with filter paper, washing with ethanol and deionized water several times, and drying at 105°C. The adsorbent was repeated five times for adsorption experiments. As shown in Fig. 6(a), the recovering ability was promising. In Fig. 6(b), the adsorption capacity showed a linear relationship with the times of use. With the increase in the times of use, the adsorption capacity just slightly decreased. After five times of repeated use of the adsorbent, there was no noticeable loss of adsorption performance.

4. Conclusion

The specific surface area of BC-MnO_2 was 349.65 m^2/g and the average pore size was 3.892 nm. The methylene blue removal rate of BC-MnO_2 was as high as 99.73%. The adsorption process of MnO_2 modified biochar to methylene blue in aqueous solution could be described by pesudo-second-order kinetics and Langmuir isotherm models, respectively. The equilibrium adsorption capacity of monolayer was 162.93 mg/g and the maximum adsorption capacity was 248.96 mg/g. Results indicated that the modification with manganese compounds is a promising strategy for the preparation of lignin-derived adsorbents for methylene blue in industrial effluents.

Declaration of Competing Interest

The authors declare that they have no known competing financial interests or personal relationships that could have appeared to influence the work reported in this paper.

Acknowledgment

This work was financially supported by Foundation for Young Talents in Forestry and Grassland Science and Technology Innovation (2019132610), State Key Laboratory of Biological Polysaccharide Fiber Forming and Ecological Textile (Qingdao University) (No. K2019-04), the National Natural Science Foundation of China (21706014), and China Scholarship Council (201906515031).

Appendix A. Supplementary data

Supplementary data to this article can be found online at https://doi.org/10.1016/j.jmrt.2021.03.076.

REFERENCES

[1] Novais RM, Ascensão G, Tobaldi DM, Seabra MP, Labrincha JA. Biomass fly ash geopolymer monoliths for effective methylene blue removal from wastewaters. J Clean Prod 2018;171:783–94. https://doi.org/10.1016/j.jclepro.2017.10.078.

[2] Ahmaruzzaman M, Gupta VK. Rice husk and its ash as low-cost adsorbents in water and wastewater treatment. Ind Eng Chem Res 2011;50(24):13589–613. https://doi.org/10.1021/ie201477c.

[3] Bedin KC, Souza IPAF, Cazetta AL, Spessato L, Ronix A, Almeida VC. CO_2-spherical activated carbon as a new adsorbent for Methylene Blue removal: kinetic, equilibrium and thermodynamic studies. J Mol Liq 2018;269:132–9. https://doi.org/10.1016/j.molliq.2018.08.020.

[4] Yang X, Jin D, Zhang M, Wu P, Jin H, Li J, et al. Fabrication and application of magnetic starch-based activated hierarchical porous carbon spheres for the efficient removal of dyes from water. Mater Chem Phys 2016;174:179–86. https://doi.org/10.1016/j.matchemphys.2016.02.073.

[5] Zhao G, Li C, Wu X, Yu J, Jiang X, Hu W, et al. Reduced graphene oxide modified NiFe-calcinated layered double hydroxides for enhanced photocatalytic removal of methylene blue. Appl Surf Sci 2018;434:251–9. https://doi.org/10.1016/j.apsusc.2017.10.181.

[6] Huang D, Ma J, Fan C, Wang K, Zhao W, Peng M, et al. Co-Mn-Fe complex oxide catalysts from layered double hydroxides for decomposition of methylene blue: role of Mn. Appl Clay Sci 2018;152:230–8. https://doi.org/10.1016/j.clay.2017.11.018.

[7] Zhang Y, Liu J, Du X, Shao W. Preparation of reusable glass hollow fiber membranes and methylene blue adsorption. J Eur Ceram Soc 2019;39(15):4891–900. https://doi.org/10.1016/j.jeurceramsoc.2019.06.038.

[8] Jorfi S, Barzegar G, Ahmadi M, Darvishi Cheshmeh Soltani R, Alah Jafarzadeh Haghighifard N, Takdastan A, et al. Enhanced coagulation-photocatalytic treatment of Acid red 73 dye and real textile wastewater using UVA/synthesized MgO nanoparticles. J Environ Manag 2016;177:111–8. https://doi.org/10.1016/j.jenvman.2016.04.005.

[9] Liu Y, Yang Z-H, Song P-P, Xu R, Wang H. Facile synthesis of $Bi_2MoO_6/ZnSnO_3$ heterojunction with enhanced visible light photocatalytic degradation of methylene blue. Appl Surf Sci 2018;430:561–70. https://doi.org/10.1016/j.apsusc.2017.06.231.

[10] Hama Aziz KH, Mahyar A, Miessner H, Mueller S, Kalass D, Moeller D, et al. Application of a planar falling film reactor for decomposition and mineralization of methylene blue in the aqueous media via ozonation, Fenton, photocatalysis and non-thermal plasma: a comparative study. Process Saf Environ Protect 2018;113:319–29. https://doi.org/10.1016/j.psep.2017.11.005.

[11] Tunç S, Gürkan T, Duman O. On-line spectrophotometric method for the determination of optimum operation parameters on the decolorization of Acid Red 66 and Direct Blue 71 from aqueous solution by Fenton process. Chem Eng J 2012;181-182:431–42. https://doi.org/10.1016/j.cej.2011.11.109.

[12] Tunç S, Duman O, Gürkan T. Monitoring the decolorization of Acid Orange 8 and Acid Red 44 from aqueous solution using Fenton's reagents by online spectrophotometric method: effect of operation parameters and kinetic study. Ind Eng Chem Res 2013;52(4):1414–25. https://doi.org/10.1021/ie302126c.

[13] Lacasa E, Cañizares P, Walsh FC, Rodrigo MA, Ponce-de-León C. Removal of methylene blue from aqueous solutions using an Fe^{2+} catalyst and in-situ H_2O_2 generated at gas diffusion cathodes. Electrochim Acta 2019;308:45–53. https://doi.org/10.1016/j.electacta.2019.03.218.

[14] Mouni L, Belkhiri L, Bollinger J-C, Bouzaza A, Assadi A, Tirri A, et al. Removal of Methylene Blue from aqueous solutions by adsorption on Kaolin: kinetic and equilibrium studies. Appl Clay Sci 2018;153:38–45. https://doi.org/10.1016/j.clay.2017.11.034.

[15] Wang Y, Pan J, Li Y, Zhang P, Li M, Zheng H, et al. Methylene blue adsorption by activated carbon, nickel alginate/activated carbon aerogel, and nickel alginate/graphene oxide aerogel: a comparison study. J Mater Res Technol 2020;9(6):12443–60. https://doi.org/10.1016/j.jmrt.2020.08.084.

[16] Chen B, Yang Z, Ma G, Kong D, Xiong W, Wang J, et al. Heteroatom-doped porous carbons with enhanced carbon dioxide uptake and excellent methylene blue adsorption capacities. Microporous Mesoporous Mater 2018;257:1–8. https://doi.org/10.1016/j.micromeso.2017.08.026.

[17] Pereira MFR, Soares SF, Órfão JJM, Figueiredo JL. Adsorption of dyes on activated carbons: influence of surface chemical groups. Carbon 2003;41(4):811–21. https://doi.org/10.1016/S0008-6223(02)00406-2.

[18] Nasrullah A, Saad B, Bhat AH, Khan AS, Danish M, Isa MH, et al. Mangosteen peel waste as a sustainable precursor for high surface area mesoporous activated carbon: characterization and application for methylene blue removal. J Clean Prod 2019;211:1190–200. https://doi.org/10.1016/j.jclepro.2018.11.094.

[19] Faizal A, Sembada AA, Priharto N. Production of bioethanol from four species of duckweeds (Landoltia punctata, Lemna aequinoctialis, Spirodela polyrrhiza, and Wolffia arrhiza) through optimization of saccharification process and fermentation with Saccharomyces cerevisiae. Saudi J Biol Sci 2020. https://doi.org/10.1016/j.sjbs.2020.10.002.

[20] David AN, Sewsynker-Sukai Y, Sithole B, Gueguim Kana EB. Development of a green liquor dregs pretreatment for enhanced glucose recovery from corn cobs and kinetic assessment on various bioethanol fermentation types. Fuel 2020;274. https://doi.org/10.1016/j.fuel.2020.117797.

[21] Singh SK. Biological treatment of plant biomass and factors affecting bioactivity. J Clean Prod 2021;279:123546. https://doi.org/10.1016/j.jclepro.2020.123546.

[22] Saka S, Bae HJ. Secondary xylem for bioconversion. Secondary Xylem Biology 2016:213–31.

[23] Jiao GJ, Ma J, Li Y, Jin D, Guo Y, Zhou J, et al. Enhanced adsorption activity for phosphate removal by functional lignin-derived carbon-based adsorbent: optimization, performance and evaluation. Sci Total Environ 2020:143217. https://doi.org/10.1016/j.scitotenv.2020.143217.

[24] Supanchaiyamat N, Jetsrisuparb K, Knijnenburg JTN, Tsang DCW, Hunt AJ. Lignin materials for adsorption: current trend, perspectives and opportunities. Bioresour Technol 2019;272:570–81. https://doi.org/10.1016/j.biortech.2018.09.139.

[25] Brazil TR, Gonçalves M, Junior MSO, Rezende MC. A statistical approach to optimize the activated carbon production from Kraft lignin based on conventional and microwave processes. Microporous Mesoporous Mater 2020;308. https://doi.org/10.1016/j.micromeso.2020.110485.

[26] Ruthiraan M, Abdullah EC, Mubarak NM, Noraini MN. A promising route of magnetic based materials for removal of cadmium and methylene blue from waste water. J Environ Chem Eng 2017;5(2):1447–55. https://doi.org/10.1016/j.jece.2017.02.038.

[27] Wang D, Li G, Zhang C, Wang Z, Li X. Nickel nanoparticles inlaid in lignin-derived carbon as high effective catalyst for lignin depolymerization. Bioresour Technol 2019;289:121629. https://doi.org/10.1016/j.biortech.2019.121629.

[28] Xu Y, Song Z, Chang X, Guo Z, Gao M. Effects of Fe-Mn oxide-modified biochar composite applications on phthalate esters (PAEs) accumulation in wheat grains and grain quality under PAEs-polluted brown soil. Ecotoxicol Environ Saf 2021:208. https://doi.org/10.1016/j.ecoenv.2020.111624.
[29] Zhai R, Hu J, Chen X, Xu Z, Wen Z, Jin M. Facile synthesis of manganese oxide modified lignin nanocomposites from lignocellulosic biorefinery wastes for dye removal. Bioresour Technol 2020;315:123846. https://doi.org/10.1016/j.biortech.2020.123846.
[30] He Y, Wang Y, Hu J, Wang K, Zhai Y, Chen Y, et al. Photocatalytic property correlated with microstructural evolution of the biochar/ZnO composites. J Mater Res Technol 2021. https://doi.org/10.1016/j.jmrt.2021.01.077.
[31] Zhu S, Xu J, Kuang Y, Cheng Z, Wu Q, Xie J, et al. Lignin-derived sulfonated porous carbon from cornstalk for efficient and selective removal of cationic dyes. Ind Crop Prod 2021;159. https://doi.org/10.1016/j.indcrop.2020.113071.
[32] Zhou Q, Liao B, Lin L, Qiu W, Song Z. Adsorption of Cu(II) and Cd(II) from aqueous solutions by ferromanganese binary oxide-biochar composites. Sci Total Environ 2018;615:115–22. https://doi.org/10.1016/j.scitotenv.2017.09.220.
[33] Chen L, Jiang X, Xie R, Zhang Y, Jin Y, Jiang W. A novel porous biochar-supported Fe-Mn composite as a persulfate activator for the removal of acid red 88. Separ Purif Technol 2020:250. https://doi.org/10.1016/j.seppur.2020.117232.
[34] Song Z, Lian F, Yu Z, Zhu L, Xing B, Qiu W. Synthesis and characterization of a novel MnO_x-loaded biochar and its adsorption properties for Cu^{2+} in aqueous solution. Chem Eng J 2014;242:36–42. https://doi.org/10.1016/j.cej.2013.12.061.
[35] Su Q, Pan B, Wan S, Zhang W, Lv L. Use of hydrous manganese dioxide as a potential sorbent for selective removal of lead, cadmium, and zinc ions from water. J Colloid Interface Sci 2010;349(2):607–12. https://doi.org/10.1016/j.jcis.2010.05.052.
[36] Asfaram A, Ghaedi M, Agarwal S, Tyagi I, Kumar Gupta V. Removal of basic dye Auramine-O by ZnS:Cu nanoparticles loaded on activated carbon: optimization of parameters using response surface methodology with central composite design. RSC Adv 2015;5(24):18438–50. https://doi.org/10.1039/c4ra15637d.
[37] Ho YS, McKay G. Pseudo-second order model for sorption processes. Process Biochem 1999;34:451–65. https://doi.org/10.1016/S0032-9592(98)00112-5.
[38] Langmuir I. The constitution and fundamental properties of solids and liquids. J Am Chem Soc 1916;38(11):2221–95. https://doi.org/10.1021/ja02268a002.
[39] Ghaedi M, Hajjati S, Mahmudi Z, Tyagi I, Agarwal S, Maity A, et al. Modeling of competitive ultrasonic assisted removal of the dyes-Methylene blue and Safranin-O using Fe_3O_4 nanoparticles. Chem Eng J 2015;268:28–37. https://doi.org/10.1016/j.cej.2014.12.090.
[40] Dil EA, Ghaedi M, Ghaedi AM, Asfaram A, Goudarzi A, Hajati S, et al. Modeling of quaternary dyes adsorption onto ZnO–NR–AC artificial neural network: analysis by derivative spectrophotometry. J Ind Eng Chem 2016;34:186–97. https://doi.org/10.1016/j.jiec.2015.11.010.
[41] Singh SK, Dhepe PL. Isolation of lignin by organosolv process from different varieties of rice husk: understanding their physical and chemical properties. Bioresour Technol 2016;221:310–7. https://doi.org/10.1016/j.biortech.2016.09.042.
[42] Guadix-Montero S, Sankar M. Review on catalytic cleavage of C-C inter-unit linkages in lignin model compounds: towards lignin depolymerisation. Top Catal 2018;61(3):183–98. https://doi.org/10.1007/s11244-018-0909-2.
[43] Feng N-c, Fan W, Zhu M-l, Guo X-y. Adsorption of Cd^{2+} in aqueous solutions using $KMnO_4$-modified activated carbon derived from Astragalus residue. Trans Nonferrous Met Soc China 2018;28(4):794–801. https://doi.org/10.1016/s1003-6326(18)64712-0.
[44] Jin Y, Zeng C, Lu QF, Yu Y. Efficient adsorption of methylene blue and lead ions in aqueous solutions by 5-sulfosalicylic acid modified lignin. Int J Biol Macromol 2019;123:50–8. https://doi.org/10.1016/j.ijbiomac.2018.10.213.
[45] Sahu S, Pahi S, Tripathy S, Singh SK, Behera A, Sahu UK, et al. Adsorption of methylene blue on chemically modified lychee seed biochar: dynamic, equilibrium, and thermodynamic study. J Mol Liq 2020;315. https://doi.org/10.1016/j.molliq.2020.113743.
[46] Li Z, Wang G, Zhai K, He C, Li Q, Guo P. Methylene blue adsorption from aqueous solution by loofah sponge-based porous carbons. Colloid Surface Physicochem Eng Aspect 2018;538:28–35. https://doi.org/10.1016/j.colsurfa.2017.10.046.
[47] Li Z, Xing B, Ding Y, Li Y, Wang S. A high-performance biochar produced from bamboo pyrolysis with in-situ nitrogen doping and activation for adsorption of phenol and methylene blue. Chin J Chem Eng 2020. https://doi.org/10.1016/j.cjche.2020.03.031.
[48] Shen Q, Wang Z, Yu Q, Cheng Y, Liu Z, Zhang T, et al. Removal of tetracycline from an aqueous solution using manganese dioxide modified biochar derived from Chinese herbal medicine residues. Environ Res 2020;183:109195. https://doi.org/10.1016/j.envres.2020.109195.
[49] Guo D, Li Y, Cui B, Hu M, Luo S, Ji B, et al. Natural adsorption of methylene blue by waste fallen leaves of Magnoliaceae and its repeated thermal regeneration for reuse. J Clean Prod 2020;267. https://doi.org/10.1016/j.jclepro.2020.121903.
[50] Fan S, Wang Y, Wang Z, Tang J, Tang J, Li X. Removal of methylene blue from aqueous solution by sewage sludge-derived biochar: adsorption kinetics, equilibrium, thermodynamics and mechanism. J Environ Chem Eng 2017;5(1):601–11. https://doi.org/10.1016/j.jece.2016.12.019.
[51] Wang Y, Zhang Y, Li S, Zhong W, Wei W. Enhanced methylene blue adsorption onto activated reed-derived biochar by tannic acid. J Mol Liq 2018;268:658–66. https://doi.org/10.1016/j.molliq.2018.07.085.
[52] Ebadollahzadeh H, Zabihi M. Competitive adsorption of methylene blue and Pb(II) ions on the nano-magnetic activated carbon and alumina. Mater Chem Phys 2020;248. https://doi.org/10.1016/j.matchemphys.2020.122893.
[53] Ayranci E, Duman O. Removal of anionic surfactants from aqueous solutions by adsorption onto high area activated carbon cloth studied by in situ UV spectroscopy. J Hazard Mater 2007;148(1–2):75–82. https://doi.org/10.1016/j.jhazmat.2007.02.006.
[54] Duman O, Ayranci E. Structural and ionization effects on the adsorption behaviors of some anilinic compounds from aqueous solution onto high-area carbon-cloth. J Hazard Mater 2005;120(1–3):173–81. https://doi.org/10.1016/j.jhazmat.2004.12.030.
[55] Duman O, Ayranci E. Adsorption characteristics of benzaldehyde, sulphanilic acid, and p-phenolsulfonate from water, acid, or base solutions onto activated carbon cloth. Separ Sci Technol 2007;41(16):3673–92. https://doi.org/10.1080/01496390600915072.
[56] Ahmed MJ, Hameed BH. Insight into the co-pyrolysis of different blended feedstocks to biochar for the adsorption of organic and inorganic pollutants: a review. J Clean Prod 2020:265. https://doi.org/10.1016/j.jclepro.2020.121762.

[57] Lian F, Cui G, Liu Z, Duo L, Zhang G, Xing B. One-step synthesis of a novel N-doped microporous biochar derived from crop straws with high dye adsorption capacity. J Environ Manag 2016;176:61–8. https://doi.org/10.1016/j.jenvman.2016.03.043.

[58] Duman O, Ozcan C, Gurkan Polat T, Tunc S. Carbon nanotube-based magnetic and non-magnetic adsorbents for the high-efficiency removal of diquat dibromide herbicide from water: OMWCNT, OMWCNT-Fe_3O_4 and OMWCNT-kappa-carrageenan-Fe_3O_4 nanocomposites. Environ Pollut 2019;244:723–32. https://doi.org/10.1016/j.envpol.2018.10.071.

[59] Ayranci E, Duman O. Structural effects on the interactions of benzene and naphthalene sulfonates with activated carbon cloth during adsorption from aqueous solutions. Chem Eng J 2010;156(1):70–6. https://doi.org/10.1016/j.cej.2009.09.038.

[60] Meili L, Lins PV, Zanta CLPS, Soletti JI, Ribeiro LMO, Dornelas CB, et al. MgAl-LDH/Biochar composites for methylene blue removal by adsorption. Appl Clay Sci 2019;168:11–20. https://doi.org/10.1016/j.clay.2018.10.012.

[61] Liu S, Li J, Xu S, Wang M, Zhang Y, Xue X. A modified method for enhancing adsorption capability of banana pseudostem biochar towards methylene blue at low temperature. Bioresour Technol 2019;282:48–55. https://doi.org/10.1016/j.biortech.2019.02.092.

[62] Ji B, Wang J, Song H, Chen W. Removal of methylene blue from aqueous solutions using biochar derived from a fallen leaf by slow pyrolysis: behavior and mechanism. J Environ Chem Eng 2019;7(3). https://doi.org/10.1016/j.jece.2019.103036.

[63] Nkutha CS, Shooto ND, Naidoo EB. Adsorption studies of methylene blue and lead ions from aqueous solution by using mesoporous coral limestones. S Afr J Chem Eng 2020;34:151–7. https://doi.org/10.1016/j.sajce.2020.08.003.

[64] Ding YH, Floren M, Tan W. Mussel-inspired polydopamine for bio-surface functionalization. Biosurf Biotribol 2016;2(4):121–36. https://doi.org/10.1016/j.bsbt.2016.11.001.

[65] Abdelrahman EA, Hegazey RM, El-Azabawy RE. Efficient removal of methylene blue dye from aqueous media using Fe/Si, Cr/Si, Ni/Si, and Zn/Si amorphous novel adsorbents. J Mater Res Technolo 2019;8(6):5301–13. https://doi.org/10.1016/j.jmrt.2019.08.051.

[66] Vadivelan V, Kumar KV. Equilibrium, kinetics, mechanism, and process design for the sorption of methylene blue onto rice husk. J Colloid Interface Sci 2005;286(1):90–100. https://doi.org/10.1016/j.jcis.2005.01.007.

[67] Zhang Z-H, Xu J-Y, Yang X-L. MXene/sodium alginate gel beads for adsorption of methylene blue. Mater Chem Phys 2020. https://doi.org/10.1016/j.matchemphys.2020.124123.